Structure of a-C:N:H prepared from ammonia

J.K. Walters, D.M. Pickup, and R.J. Newport[a)]
School of Physical Sciences, University of Kent, Canterbury CT2 7NR, United Kingdom

(Received 16 May 2005; accepted 18 August 2005)

A range of nitrogen-doped amorphous hydrogenated carbon samples (a-C:N_x:H, where $x = 3$ at.% and $x = 7$ at.%) have been studied using neutron diffraction, inelastic neutron scattering (INS) and Fourier transform infra-red (FTIR) spectroscopy to obtain detailed information about their atomic-scale structure, particularly the bonding environment of the hydrogen. The results show that the overall atomic scale network structure of the two samples is very similar; however, the hydrogen-bonding sites alter subtly as the nitrogen content of the samples is increased.

I. INTRODUCTION

A complex problem in the study of amorphous materials is determining the relationship between the atomic-scale structure and the macroscopic properties of a material, the solution of which maintains amorphous materials in a position of both fundamental and technological interest. An example of such a material is diamondlike carbon (DLC). It is of technological interest because it can be prepared harder, denser, and more resistant to chemical attack than any other solid hydrocarbon,[1,2] which, together with a high degree of transparency to the infrared and histocompatibility, have led to many applications.[3,4] Hydrogenated or nitrogenated DLC films are used in hard-disk drive applications as protective overcoats on media and sliders[5] and continue to be studied in connection with their potential as biomaterials.[6]

Nitrogen-doped amorphous hydrogenated carbon (a-C:N:H) was first prepared in 1982 by Jones and Stewart.[7] The motivations behind the addition of nitrogen to a-C:H primarily stemmed from the possible modifications to its electronic properties, and the possibility of their technological applications. The similar sizes of carbon and nitrogen atoms, coupled with the relative ease of sample preparation, makes doping with nitrogen an obvious choice, although a variety of other dopant atoms have been tried (for example, Refs. 7 and 8). Since that time, much experimental work has been carried out on a-C:N:H. Many studies have focused on the optical and electronic properties of the material,[7–13] with additional interest arising from the fact that it may form a phase harder than undoped a-C:H.[14] Structural investigations hitherto have mainly involved infrared and Raman spectroscopy studies,[15–27] although other methods, such as photoemission and x-ray absorption near edge sspectroscopy (XANES) have been applied with varying degrees of success.[22–24,28–30]

Because of the possible technological applications of these properties, and certainly from a fundamental point of view, it is important to examine the effects of nitrogen incorporation by probing the atomic structure of this material.

Building on our work on a-C:H[31,32] and earlier studies on a-C:N:H,[33,34] we present complementary neutron diffraction, inelastic neutron scattering and infrared spectroscopy data for a-C:N:H samples, with compositions of 3 and 7 at.% nitrogen, which will be used to provide additional insight into the carbon, nitrogen, and hydrogen bonding environments present. In particular, we examine the effects of nitrogen incorporation on the atomic-scale structure of the material with reference to the use of ammonia, NH_3, as the source of nitrogen, and a supplementary source of hydrogen, in the precursor gas. In this context, it is important to note that the choice of precursor materials and the nature of, and parameters associated with, sample synthesis may have a significant effect on the resultant material, both in terms of its bulk properties and with respect to its atomic-scale structure (e.g., Refs. 30, 35, and 36). Thus, while the generic knowledge gained by the many researchers studying this family of materials worldwide is of great importance, it must be used with circumspection in the interpretation of particular data sets.

Diffraction experiments provide an opportunity to obtain direct information on interatomic distances and on the average numbers of atoms in each coordination shell. Previously, a-C:N:H has been studied using electron diffraction[8] and neutron and x-ray diffraction.[33] Neutron diffraction has already been established as a powerful technique in the study of amorphous materials (see, for example Refs. 31, 37, and 38) and in particular the pulsed neutron source ISIS at the Rutherford Appleton Laboratory (Didcot, UK) allows one to obtain high-resolution real-space data, to the extent that it is possible to

[a)]Address all correspondence to this author.
e-mail: r.j.newport@kent.ac.uk
DOI: 10.1557/JMR.2005.0423

distinguish sp^1, sp^2, and sp^3 carbon-bonding environments directly.[31] Furthermore, because the neutron, unlike x-rays or electrons, scatters from the nucleus, there is no atomic-number-dependent form factor, and the correlations involving hydrogen are also accessible.

Infrared (IR) spectroscopy is a widely used technique in the study of materials based upon the a-C:H system, e.g., Refs. 39–41, especially for investigating the hydrogen bonding environment. In their seminal work, Dischler et al.[39] performed an extensive study of the bonding of hydrogen in a-C:H and proposed assignments for all the observed frequencies. Also, Vandentrop et al.[41] used IR spectroscopy to estimate CH_2:CH_3 ratios, but all IR results necessarily depend upon assumptions for the matrix elements of each vibration, making fully quantitative analysis very difficult. The technique has, however, been used quite successfully to look at trends between different samples.[34,42] In the specific context of the family of materials based upon ta-C:N, a-C:N:H, and similar materials, a comprehensive overview and discussion is offered by Ferrari et al.[43] IR spectroscopy data may become even more important as computer simulations are able to generate spectra to compare with experimental data.[44]

Inelastic neutron scattering (INS) does not suffer from this problem as the observed scattering intensity is directly related to the eigenvector of the vibration, although the energy resolution is not as good as for IR spectra. In addition, there are no forbidden transitions in the INS case. INS data is most useful for looking at the region of low energy vibrations (~400–1800 cm^{-1}, i.e., ~50–225 meV), which includes the modes associated with CH_2 and CH_3 deformations and carbon–carbon stretches.

Thus, a combination of these three experimental methods—neutron diffraction (interatomic distances), IR (frequencies and relative peak intensities), and INS (low frequencies and peak intensities)—enable the relative proportions and assignments of different bonding environments to be determined with a higher degree of reliability.

II. EXPERIMENTAL DETAILS AND DATA ANALYSIS

A. Sample preparation

The samples were prepared using a saddle field fast-atom (i.e., neutral particle) source[45,46] from acetylene and ammonia precursor gases. The samples were prepared at a deposition pressure of ~10^{-4} mbar. To incorporate nitrogen into the samples, ammonia gas was simply fed into the source with the acetylene using two preset and controlled flow rates. The experimental techniques require samples in the form of powders, and this is achieved by depositing the material as a thin film onto a copper substrate, previously cleaned with argon. Since copper carbide does not readily form, the compressive stresses within the thin film soon cause it to detach from the substrate, and as it falls, the powder sample is collected. The compositions of the samples were determined by Carlo–Erba CHN combustion analysis. The results of these measurements together with the deposition energies used, are summarized in Table I.

B. Neutron diffraction

The data presented here were collected using the SANDALS diffractometer[47] at the pulsed neutron facility, ISIS, at the Rutherford Appleton Laboratory. This instrument is particularly well-suited to the study of covalently bonded amorphous materials, allowing the collection of data over a wide dynamic range (~0.2–50 $Å^{-1}$). It is also optimized for looking at hydrogenous samples by collecting data only at forward-scattering angles to reduce the effects of inelastic scattering. This is discussed more fully in the data analysis section.

Neutrons are scattered from the sample into fixed-angle detectors (i.e., at a given scattering angle 2θ), where the scattered intensity is measured as a function of time of flight (tof, which can be directly related to the neutron's momentum transfer on scattering). The complete scattering profile is then obtained by combining overlapping spectra form different detector angles. Monitors record the tof spectra of the incident and transmitted beams to provide information on the total neutron cross-section and the intensity:wavelength profile of the incident beam. For each experiment, measurements are required for the sample, the empty sample container, a background without sample or container, and a vanadium rod of comparable geometry to the sample and container. The vanadium rod measurement allows the sample scattering to be put on an absolute scale, since vanadium has a well-known and almost entirely incoherent scattering cross-section.[48]

TABLE I. Compositional information about the samples derived from combustion analysis.

Sample	Mass flow ratio of precursor gases acetylene:ammonia	C content (at.%)	N content (at.%)	H content (at.%)	Deposition energy (eV)
1	2:1	75	3	22	850
2	1:1	69	7	24	850

In a neutron scattering experiment, the aim is to determine a structure factor $S(Q)$, where, for an amorphous material (i.e., an isotropic scatterer),[48]

$$S(Q) = 1 + \frac{4\pi\rho}{Q}\int_0^\infty r dr[g(r) - 1]\sin(Qr) \quad ,$$

where ρ is the average number density of atoms in the material; $Q = |Q| = |k_i - k_f|$ is the wavevector transfer associated with the diffraction experiment for elastic scattering from a liquid or amorphous solid, $Q = 4\pi/\lambda\sin\theta$, where 2θ is the scattering angle and λ is the neutron wavelength; and $g(r)$ is called the pair correlation function, which is a measure of the atomic density at a distance r from a given origin atom. The pair correlation function may be obtained by Fourier transformation of the structure factor, which is directly related to the measured neutron scattering intensity. For a tertiary system such as a-C:N:H, each atom-type pair contributes to the total structure factor; i.e., six independent pairwise contributions are combined to give the total structure factor, each contribution being weighted according to the appropriate scattering cross sections and concentrations of the pair of elements responding real-space function, the total pair correlation function $G(r)$ is a weighted combination of the partial pair correlation functions and is defined (according to the Faber–Ziman formalism[48]) as

$$G(r) = \sum_{\alpha\beta}[c_\alpha c_\beta b_\alpha b_\beta g_{\alpha\beta}z(r)] \quad ,$$

where c_α is the atomic fraction and b_α the coherent scattering length, both of element α, and $g_{\alpha\beta}(r)$ represents the partial terms in $G(r)$ and describe the probability of finding an atom of type β at a distance r from an atom of type α at the origin. The weighting coefficients of the partials means that for these samples the dominant terms are those arising from CC, CN, and CH correlations, with CH and NH correlations appearing as troughs rather than peaks since b_H is negative (due to the π-phase shift experienced by a neutron scattering from hydrogen). Note that the CH and HC, NH and HN, etc., terms are equivalent.

The equations above rely on the static approximation[49,50] being valid, i.e., that the change in the neutron's energy on scattering is small compared to its incident energy. Corrections need to be applied to the data before the structure factor can be generated. The major corrections are for background, container and multiple scattering, attenuation, and the effects of inelastic scattering (that is, for deviations from the static approximation). Full details of these may be found elsewhere.[51] The most problematic step in the analysis procedure is the correction for inelastic scattering. Although the small angle neutron diffractometer for amorphous and liquid samples instrument has been designed to minimize the effects of this on the experimental data, it is by no means completely eliminated. For hydrogenous materials, the simplistic approaches[52] to accounting for this deviation from purely elastic scattering (i.e., from the static approximation) break down because of the low mass and high incoherent scattering cross section of the hydrogen atom, and an alternative method has to be used. The method adopted here is an empirical one, which involves fitting a low-order polynomial through the data to remove the underlying incoherent scattering curve; to first order the effects of inelastic scattering are embedded in this term. The procedure for performing this correction is given in detail elsewhere.[53] There are problems with using this approach, particularly with regard to the quality of the data at very low r values (below ~1 Å), which may affect correlation amplitudes. Therefore, we expect peak areas, and to a far lesser extent bond distances, for correlations involving hydrogen first coordination shells to be subject to larger uncertainties than pertain to the bulk of the data.

C. IR spectroscopy

IR measurements were performed using a Bio-Rad FTS 175C dynamic alignment Fourier transform infrared spectrometer fitted with a photo-acoustic detector. Given the intrinsic difficulties associated with any attempt to analyze IR data quantitatively, we concentrate here on using Gaussian peak fits to the fundamental C–H stretch modes to examine the overall nature of the hydrogen bonding environment and its variation between different samples. The peak fitting is constrained to peaks at the known vibrational frequencies for C–H stretching modes in this region.

D. Inelastic neutron scattering

The INS data was collected on the incoherent inelastic neutron spectroscopy instrument at the ISIS spallation source, Rutherford Appleton Laboratory.[47] The data presented in this paper were derived from an experiment on the ISIS time focused crystal analyzer spectrometer, TFXA, which was optimized for energy resolution ($\Delta E/E \sim 1.5\%$ to 3%, with a low associated Q resolution resulting from the integration needed to achieve the desired high count rates. The TFXA spectrometer has since been replaced by the instrument TOSCA, which has an even higher specification[54]). This spectrometer is used to collect the H-dominated incoherent INS data, where it generates high intensity data integrated over momentum transfer. In the incoherent approximation,[55] the scattering function can be directly related to the vibrational density of states $g(\omega)$:

$$S^s(Q,\omega) = \frac{\hbar Q^2}{2m}e^{-2W}\frac{(1 + \langle n_\lambda\rangle)}{\omega}g(\omega) \quad ,$$

where $S^S(Q,\omega)$ is the self scattering, $\hbar Q$ is the momentum transfer, $\hbar\omega$ the energy transfer, $\langle n_\lambda \rangle$ is the population factor for a mode of frequency ω_λ and e^{-2W} is the Debye–Waller factor. A more complete account of the theory is given elsewhere.[55,56] It should be noted that in an amorphous system such as a-C:H, there is a range of possible bonding environments that give rise to vibrations over a spread of frequencies.

III. RESULTS AND DISCUSSION

A. Combustion analysis

The results from the combustion analysis of the composition of the samples show that, as the amount of ammonia in the input gas mixture is increased, there is a large decrease in the atomic concentration of carbon and a small increase in the percentage of hydrogen present in the sample. This preferential reduction in carbon content has also been observed in samples prepared using N_2 gas as the source of nitrogen in the deposition process.[17,33]

B. Neutron diffraction

The pair correlation functions $G(r)$ for the two samples are shown in Fig. 1. It is immediately apparent how similar the two sets of data are. For both samples, the combined CC and CN first neighbor peak is at 1.43 Å, which is shorter than that obtained for CC nearest neighbors in a-C:H samples.[31,33] This is due to the presence of CN and NN bonds, which are shorter than the expected C–C and C=C bonds, and therefore the average network neighbor bond distance observed for these a-C:N:H samples, where the correlation peaks overlap, appears shorter. The CH and NH correlations are observed as a dip in the data at ~1 Å. However, this region is affected by the difficulties in correcting the data for inelastic scattering, so we can say nothing more than that there is

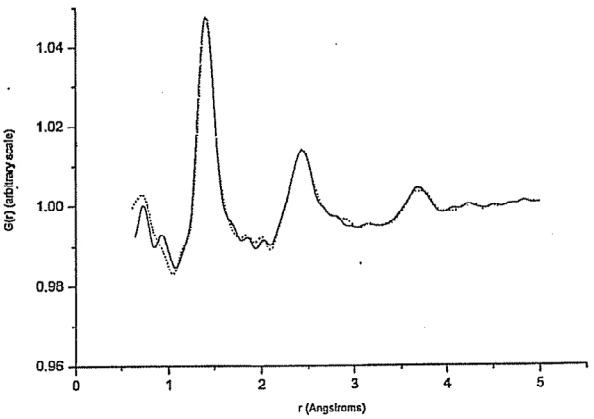

FIG. 1. Pair correlation functions $G(r)$, obtained from neutron diffraction experiments for sample 1 (dashed line) and sample 2 (solid line).

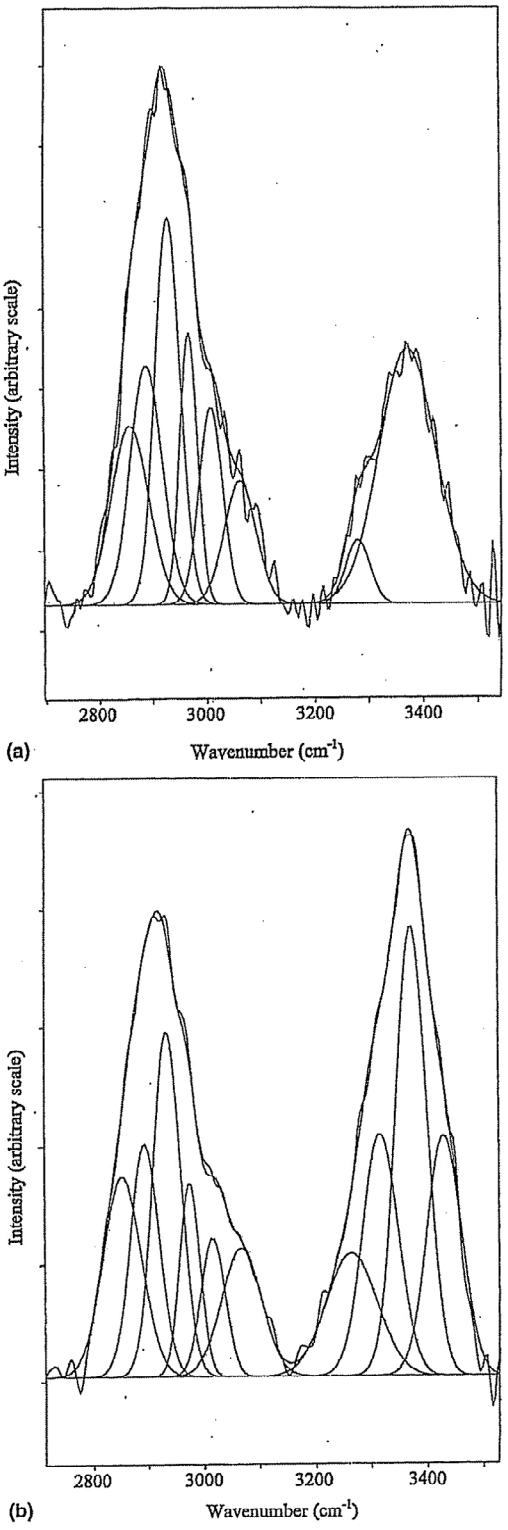

FIG. 2. (a) FTIR spectrum for sample 1 with the Gaussians used to fit the data. (b) FTIR spectrum for sample 2 with the Gaussians used to fit the data.

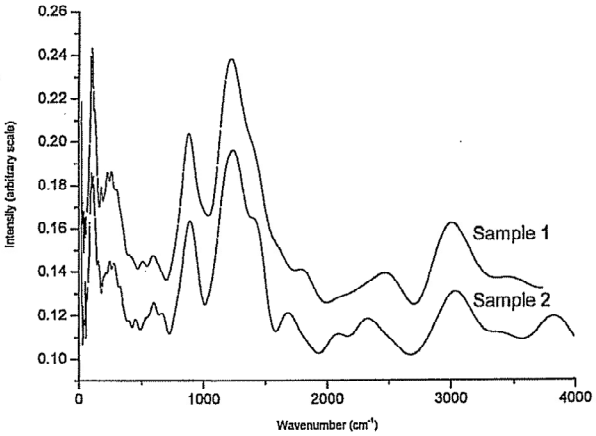

FIG. 3. Smoothed INS spectra for samples 1 and 2 (off-set).

evidence to show that the samples contain C–H and N–H bonds, as might be anticipated. The nature and relative numbers of these bonds is discussed in more detail in the next section.

C. Spectroscopy

In a detailed examination of the spectroscopic results, it is more instructive to consider two different regions of the spectra, 3400–2600 cm^{-1} (CH stretch region) and 1800–10 cm^{-1} (CC stretch and CH_n deformation region) separately to begin with; we will then attempt to correlate the findings from both in a general discussion of the results. The IR spectra are shown in Fig. 2 with the Gaussian peaks used to fit the data, and the INS spectra are shown in Fig. 3.

1. CH stretch region: 3400–2600 cm^{-1}

Due to the poor resolution of the INS data in this region (300–500 meV), only IR data are discussed for the CH stretching modes. Following a "background subtraction" using a low order polynomial, each spectrum is fitted with a series of Gaussians, allowing the area to vary and using the method of least squares until a best fit is found, but with the position constrained to known CH vibrational frequencies. From the positions of the Gaussians, assignment of the observed frequencies to particular vibrational modes can be made, and the peak areas can be normalized to the hydrogen content of the sample and used to look at the relative proportions of each mode present in the samples. Table II gives the frequency and associated normalized peak areas derived from this data.

If we assume that the peaks associated with the antisymmetric and symmetric stretching modes for the same group have the same area, it is possible to determine the relative numbers of sp^3CH_3, sp^3CH_2, sp^3CH, and sp^2CH groups, and these are shown in Table III. It is important to remember that these values are not absolute; comparisons are meaningful only in a relative way between samples.

Before discussing the results in detail, it is worth pointing out that although frequencies for sp^2CH_2 groups are not observed (they are not clearly observed in IR spectra for a-C:H in general, e.g., Refs. 57–59), this is due to the weightings of their matrix elements and does not necessarily imply that these groups are absent from the amorphous material structure. From Fig. 2 and Table II, it is clear that there are several frequency assignments common to all of the samples, each of which can be assigned to different CH_n vibrations.

As the ammonia content of the precursor gas is increased, there are some changes in the hydrogen bonding environments: the amount of sp^3CH_3 decreases; however, sp^3CH_2 and N–H stretching modes are both seen to increase. These changes in the C–H bonding environments are opposite those observed when N_2 is used as the precursor gas.[34]

2. CC, NN, CH, and NH stretch regions and the CH_n deformation region: 0–4000 cm^{-1}

For the CC stretch and CH_n deformation region of the spectrum, INS experiments are the best source of structural information, although the intensities at the low energy transfer values are more difficult to interpret. The general assignments for this region are: 800–100 cm^{-1} sp^2C–H out-of-plane and in-plane bending, 1100–1300 cm^{-1} sp^3C–C stretch, and –CH_2 wag/twist, 1300–1500 cm^{-1} sp^3CH_2 and CH_3 deformations, 1500–1700 cm^{-1} $sp^2C=C$ and aromatic C=C stretches,

TABLE II. Results of the Gaussian fitting to the infrared spectra.

Sample	N (at.%)	Peak position (cm^{-1}) (Normalized peak area)					
1	3	2857	2888	2929	2967	3007	3062
		(0.17)	(0.22)	(0.23)	(0.14)	(0.10)	(0.13)
2	7	2852	2888	2934	2974	3015	3066
		(0.21)	(0.18)	(0.26)	(0.11)	(0.09)	(0.14)
Assignment		sp^3CH_2	sp^3CH_3	sp^3CH_2 + sp^3CH	sp^3CH_3	sp^2CH	arom sp^2C–H

TABLE III. Relative proportions of CH_n groups from Gaussian fitting to the C–H stretch region of the infrared data.

Sample	N (at.%)	sp^3CH_3	sp^3CH_2	sp^3CH	sp^2CH
1	3	0.14	0.17	0.06	0.10
2	7	0.11	0.21	0.05	0.09

2070 cm^{-1} C≡N stretch, 3000 cm^{-1} C–H stretch and ~3300 cm^{-1} NH_2 stretch. Intensity in the region 0–400 cm^{-1} is generally due to vibrations of large fragments of the lattice/network. The smoothed INS spectra in Fig. 3 show that these bands are common to all samples. We have been able to fit smoothed spectra for the two samples with a series of Gaussians, in the same way that the IR spectra are fitted (shown in Fig. 2). The fitted peak positions and normalized peak areas are presented in Table IV. Although it is not possible to be more specific in our peak assignments, it is easier to examine and discuss the trends between different data sets. Notice that a similar collection of Gaussians is used to fit each sample, showing that the features in the data are consistent between samples. However, there are also regions where the spectra show significant differences with increasing N concentration. The regions of the data will now be discussed separately in detail:

a. 800–900 cm^{-1}: sp^2C–H in-plane and out-of-plane bending

In this region, the two spectra look very similar. However, it is interesting to contrast these spectra with that obtained for a-C:H.[32] There is clearly a peak in these samples at around 900 cm^{-1}, which does not appear separately in the a-C:H samples. This separation is probably due to the absence of the CH_2 wag intensity at ~1000 cm^{-1} in the NH_3-prepared samples. Although the IR data show a relative increase in the CH_2 groups between the two samples, it is clear from the INS spectra that there are fewer CH_2 groups in these samples than in a-C:H samples. Even with N_2-prepared samples, the CH_2 wag intensity remains. This immediately reveals that preparing samples with NH_3 affects the distribution of hydrogen within the network, in agreement with other observations.[20,43]

b. ~1250 cm^{-1}: sp^3C–C stretching

This peak is common to both samples with approximately the same shape and intensity for each one. So, for materials synthesized using the method adopted herein, the concentration of sp^3C–C bonds appears to remain constant when the N-doping of the samples is increased.

c. ~1450 cm^{-1}: CH_2 and CH_3 deformations

In both samples, this peak is present as a shoulder on the sp^3C–C peak. In sample 2, with the higher N content, this shoulder is slightly better resolved from the main C–C peak, although the intensity remains the same as for sample 1. The enhanced definition of the peak may be due to the decrease in CH_3 groups as observed in the IR data and the corresponding increase in the number of sp^3CH_2 groups.

d. ~1500–1800 cm^{-1}: sp^2C=C stretching, C=N and N=N stretching, and others

This region of the spectrum is generally difficult to interpret because it may also contain some overtone and combination modes. However, it is clear that there are differences in the spectra for the two samples presented here. In sample 1, with the lower N-content, there are two peaks at 1570 and 1816 cm^{-1}, whereas for sample 2 there is just one peak at 1693 cm^{-1}. This change shows that there is some change in sp^2 bonding in the network, but it is difficult to be more specific about the precise nature of these changes.

e. ~1800–4000 cm^{-1}

Again, it is difficult to make accurate peak assignments in this region because of overtone and combination modes. There is a peak at ~2070 cm^{-1}, which is likely to be due to C≡N stretches and shows a small increase in intensity with increasing N concentration. This increase has also been found in other IR data.[15,17,60] There is movement of the peak at 2480–2337 cm^{-1}, but this cannot be assigned to a specific bonding environment. Finally, we can assign the peak at ~3000 cm^{-1} to C–H stretches with approximately the same position and

TABLE IV. Results of the Gaussian fitting to the INS spectra.

Sample	N (at.%)	Peak position (cm^{-1}) (Normalized peak area)										
1	3	108 (54)		888 (162)	1224 (251)	1420 (150)	1572 (251)	1816 (170)	2070 (56)	2480 (310)	2997 (278)	3290 (491)
2	7	106 (51)	606 (177)	886 (151)	1229 (256)	1439 (141)	1693 (190)		2074 (125)	2337 (310)	3025 (290)	3365 (400)
Assignment				sp^2CH	sp^3CC	CH_2 +CH_3 def	NH_2 bend	C=C str	C≡N str		C–H str	NH_2 str

intensity for both samples, and then there is a small peak in both samples at ~3300 cm^{-1}, which we can assign to NH_2 stretches.[15,17]

f. 0–700 cm^{-1}

This region is generally associated with vibrations of large fragments of the network. There are small differences between the two spectra in this region of the data. However, assignment to specific vibrations is not possible, and one may draw only the general conclusion that the intermediate range order associated with the amorphous network structure has been only slightly affected by the incorporation of N.

IV. CONCLUSIONS

It is clear from all three sets of data that the samples have a very similar basic network structure despite a significant change in the nitrogen doping level. In fact, the only differences between the two samples seem to be concerned with the bonding environment of the hydrogen. It appears that using NH_3 as a precursor gas results in a general increase in the number of N–H bonds and a corresponding decrease in the number of C–H bonds, particularly in the number of CH_3 groups, when compared to samples deposited using N_2 as the source of nitrogen in the precursor gas mix. This provides clear evidence for the direct effect of nitrogen on the connectivity of the atomic-scale structure via an alteration in the distribution of network-terminating hydrogens. These conclusions are broadly in accord with the results of work by other authors.

ACKNOWLEDGMENTS

We wish to thank Dr. M.A. Holland for his help in gathering some of the FTIR data, and Dr. W.S. Howells and Dr. S.F. Parker for their supportive contribution in the context of neutron scattering experiments. We are grateful to the Council for the Central Laboratory of the Research Councils for providing access to the ISIS pulsed neutron source, and the University of Kent for provision of laboratory facilities.

REFERENCES

1. J.C. Angus, P. Koidl, and S. Domitz: Carbon thin films, in *Plasma Deposited Thin Films,* edited by J. Mort and F. Jansen (Chemical Rubber Company Press, Boca Raton, FL, 1989), p. 89.
2. J. Robertson: Amorphous carbon. *Adv. Phys.* **35,** 317 (1986).
3. A.H. Lettington: Applications of diamond-like carbon thin films. *Carbon* **36,** 555 (1998).
4. F.M. Kimock and B.J. Knapp: Commercial applications of ion-beam deposited diamond-like carbon (DLC) coatings. *Surf. Coat. Technol.* **56,** 273 (1993).
5. D. Debajyoti, K.H. Chen, S. Chattopadhyay, and L.C. Chen: Spectroscopic studies of nitrogenated amorphous carbon films prepared by ion beam sputtering. *J. Appl. Phys.* **91,** 4944 (2002).
6. S.E. Rodil, R. Olivares, and H. Arzate: *In vitro* cytotoxicity of amorphous carbon films. *Biomed. Mater. Eng.* **15,** 101 (2005).
7. D.I. Jones and A.D. Stewart: Properties of hydrogentated amorphous carbon films and the effects of doping. *Philos. Mag. B* **46,** 423 (1982).
8. C.A. Davis, Y. Yin, D.R. McKenzie, L.E. Hall, E. Kravtchinskaia, V. Keast, G.J. Amaratunga, and V.S. Veerasamy: The structure of boron-, phosphorus-, and nitrogen-doped tetrahedral amorphous carbon deposited by cathodic arc. *J. Non-Cryst. Solids* **170,** 46 (1994).
9. O. Amir and R. Kalish: Properties of nitrogen-doped amorphous hydrogentated carbon films. *J. Appl. Phys.* **70,** 4958 (1991).
10. A. Mansour and D. Ugolini: Photoelectron spectroscopy study of amorphous a-CN_x:H. *Phys. Rev. B* **47,** 10201 (1993).
11. D. Mendoza, J. Anguilar-Hernandez, and G. Contreras-Puente: Graphite-like bonding induced in hydrogenated amorphous carbon films with high nitrogen content. *Solid State Commun.* **84,** 1025 (1992).
12. V.S. Veerasamy, G.A.J. Amaratunga, W.I. Milne, J. Robertson, and P.J. Fallon: Influence of carbon ion energy on properties of highly tetrahedral diamond-like carbon. *J. Non-Cryst. Solids* **164-166,** 1111 (1993).
13. C.A. Davis, D.R. McKenzie, Y. Yin, E. Kravtchinskaia, G.A.J. Amaratunga, and V.S. Veerasamy: Substitutional nitrogen doping of tetrahedral amorphous carbon. *Philos. Mag. B* **69,** 1133 (1994).
14. A.Y. Liu and M.L. Cohen: Structural properties and electronic structure of low-compressibility materials: β–Si_3N_4 and hypothetical β–C_3N_4. *Phys. Rev. B* **41,** 10727 (1990).
15. H. Han and B.J. Feldman: Structural and optical properties of amorphous carbon nitride. *Solid State Commun.* **65,** 921 (1988).
16. D.F. Franceschini, C.A. Achete, F.L. Freire, W. Beyer, and G. Mariotto: Structural modifications in *a*-C:H films doped and implanted with nitrogen. *Diamond Relat. Mater.* **3,** 88 (1993).
17. J.H. Kaufman, S. Metin, and D.D. Saperstein: Symmetry breaking in nitrogen-doped amorphous carbon: Infrared observation of the Raman-active G and D bands. *Phys. Rev. B* **39,** 13053 (1989).
18. J. Viehland, S. Lin, B.J. Feldman, K. Kilgore, and M.I. Jones: Search for the nitrogen dangling bond in amorphous hydrogentated carbon nitride. *Solid State Commun.* **80,** 597 (1991).
19. D. Li, S. Lopez, Y.W. Chung, M.S. Wang, and W.D. Sproul: Ionized magnetron sputter deposition of amorphous carbon nitride thin films. *J. Vac. Sci. Technol. A* **13,** 1063 (1995).
20. N.P. Barradas, R.U.A. Khan, J.V. Anguita, S.R.P. Silva, U. Kreissig, R. Grötzschel, and W. Möller: Growth and characterisation of amorphous carbon films doped with nitrogen. *Nucl. Instrum. Meth. B* **161,** 969 (2000).
21. S.E. Rodil, A.C. Ferrari, J. Robertson, and S. Muhl: Infrared spectra of carbon nitride films. *Thin Solid Films* **420,** 122 (2002).
22. B. Bouchet-Fabre, C. Godet, M. Lacerda, S. Charvet, K. Zellama, and D. Ballutaud: Stoichiometry and infrared absorption of amorphous a-$C_{1-x}N_x$:H carbon nitride films. *J. Appl. Phys.* **95,** 3427 (2004).
23. S.E. Rodil and S. Muhl: Bonding in amorphous carbon nitride. *Diamond Relat. Mater.* **13,** 1521 (2004).
24. B. Bouchet-Fabre, K. Zellama, C. Godet, D. Ballutaud, and T. Minea: Comparative study of the structure of a-CN_x and a-CN_x:H films using NEXAFS, XPS and FT-IR analysis. *Thin Solid Films* **482,** 156 (2005).
25. G. Lazar, K. Zellama, I. Vascan, M. Stamate, I. Lazar, and I. Rusu: Infrared absorption properties of amorphous carbon films. *J Optoelectron. Adv. Mater.* **7,** 647 (2005).

26. G. Fanchini, P. Mandracci, A. Tagliaferro, S.E. Rodil, A. Vomiero, and G.D. Mea: Growth and characterisation of polymeric amorphous carbon and carbon nitride films from propane. *Diamond Relat. Mater.* **14,** 928 (2005).
27. S.E. Rodil: Infrared spectra of amorphous carbon-based materials. *Diamond Relat. Mater.* **14,** 1262 (2005).
28. J.M. Ripalda, E. Roman, N. Diaz, L. Galan, I. Montero, G. Comelli, A. Baraldi, S. Lizzit, A. Goldoni, and G. Paolucci: Correlation of x-ray absorption and x-ray photoemission spectroscopies in amorphous carbon nitride. *Phys. Rev. B* **60,** R3705 (1999).
29. A.S. Ferlauto, A. Champi, C.A. Figueroa, C.T.M. Ribeiro, F.C. Marques, and F. Alvares: Structural properties of amorphous carbon nitride films prepared by ion-beam-assisted deposition. *J. Non-Cryst. Solids* **338,** 486 (2004).
30. E. Marino, B. Bouchet-Fabre, D. Porterat, and C. Reynaud: Spectroscopic study of carbon nitride nanoparticles synthesised by laser pyrolysis. *Diamond Relat. Mater.* **14,** 1120 (2005).
31. J.K. Walters, P.J.R. Honeybone, D.W. Huxley, R.J. Newport, and W.S. Howells: The structural properties of amorphous hydrogenated carbon: I. A high resolution neutron diffraction study. *Phys. Rev. B* **50,** 831 (1994).
32. J.K. Walters, R.J. Newport, W.S. Howells, and S.F. Parker: A spectroscopic study of the structure of amorphous hydrogenated carbon. *J. Phys.: Condens. Matter* **7,** 10059 (1995).
33. J.K. Walters, R.J. Newport, W.S. Howells, and G. Bushnell-Wye: Neutron and x-ray diffraction studies of a-C:N:H. *J. Phys.: Condens. Matter* **8,** 4739 (1996).
34. J.K. Walters, M. Kühn, C. Spaeth, E. Dooryhee, and R.J. Newport: X-ray diffraction studies of the effects of N incorporation in amorphous CN_x materials. *J. Appl. Phys.* **83,** 3529 (1998).
35. G. Lazar and I. Lázar: IR characterisation of a-C:N:H films sputtered in $Ar/CH_4/N_2$ plasma. *J. Non-Cryst. Solids* **331,** 70 (2003).
36. Y. Qui and L. Gao: P-type carbon nitride synthesized by a gas-solid reaction. *J Am. Ceram. Soc.* **87,** 1598 (2004).
37. P.A.V. Johnson, A.C. Wright, and R.N. Sinclair: Neutron-scattering from vitreous silica. II. Twin-axis diffraction experiments. *J. Non-Cryst. Solids* **58,** 109 (1983).
38. P.H. Gaskell, A. Saeed, P. Chieux, and D.R. McKenzie: The structure of highly tetrahedral amorphous diamond-like carbon I. Neutron-scattering studies. *Philos. Mag. B* **66,** 155 (1992).
39. B. Dischler, A. Bubenzer, and P. Koidl: Bonding in hydrogenated hard carbon studied by optical spectroscopy. *Solid State Comm.* **48,** 105 (1983).
40. J.C. Angus, J.E. Stultz, P.J. Shiller, J.R. MacDonald, M.J. Mirtich, and S. Domitz: Composition and properties of the so-called diamond-like amorphous-carbon films. *Thin Solid Films* **118,** 311 (1984).
41. G.J. Vandentrop, M. Kawasaki, K. Kobayashi, and G.A. Somorjai: The effect of ion-energy flux on the properties of hydrogenated amorphous-carbon films. *J. Vac. Sci. Technol. A* **9,** 1157 (1991).
42. J.K. Walters, D.M. Fox, T.M. Burke, O.D. Weedon, R.J. Newport, and W.S. Howells: The effect of temperature on the structure of amorphous hydrogenated carbon. *J. Chem. Phys.* **101,** 4288 (1994).
43. A.C. Ferrari, S.E. Rodil, and J. Robertson: Interpretation of infrared and Raman spectra of amorphous carbon nitrides. *Phys. Rev. B* **67,** 155306 (2003).
44. F. Mauri and A.D. Corso: Vibrational properties of tetrahedral amorphous carbon from first principles. *Appl. Phys. Lett.* **75,** 644 (1999).
45. J. Franks: Atom beam source. *Vacuum* **34,** 259 (1984).
46. J. Franks: Preparation and properties of diamondlike-carbon films. *J. Vac. Sci. Technol. A* **7,** 2307 (1989).
47. User Guide to Experimental Facilities at ISIS, at www.isis.rl.ac.uk (Rutherford Appleton Laboratory, Didcot, U.K., 1992).
48. R.J. Newport: The structure of liquids and amorphous solids, in *Neutron Scattering at a Pulsed Source* edited by R.J. Newport, B.D. Rainford and R. Cywinski (Hilger, Bristol, U.K., 1988), p. 233.
49. G.L. Squires: Introduction to the theory of thermal neutron scattering (Cambridge University Press, Cambridge, 1978).
50. J.M.F. Gunn: Theory of neutron scattering, in *Neutron Scattering at a Pulsed Source*, edited by R.J. Newport, B.D. Rainford, and R. Cywinski (Hilger, Bristol, U.K., 1988), p. 24.
51. W.S. Howells, A.K. Soper, and A.C. Hannon: ATLAS—analysis of time-of-flight diffraction data from liquid and amorphous samples, Rutherford Appleton Laboratory Report RAL-89-046 (Rutherford Appleton Laboratory, Didcot, U.K., 1989).
52. J.G. Powles: Slow neutron scattering by molecules. *Mol. Phys.* **36,** 1181 (1978).
53. A.K. Soper and D.T. Bowron: SANDALS—Small angle neutron diffractometer for amorphous and liquid samples, at www.isis.rl.ac.uk/Disordered/SANDALS.htm, and references therein (2000).
54. S.F. Parker, C.J. Carlile, T. Pike, J. Tomkinson, R.J. Newport, C. Andreani, F.P. Ricci, F. Sacchetti, and F. Zoppi: TOSCA: A world class inelastic neutron spectrometer. *Physica B* **241–243,** 154 (1998).
55. S.W. Lovesey: *Theory of Neutron Scattering from Condensed Matter,* Vol. 1 (Clarendon Press, Oxford, U.K., 1984), pp. 257–264.
56. J. Tomkinson: Inelastic incoherent neutron scattering spectroscopy of hydrogen vibrations in metals and molecules, in *Neutron Scattering at a Pulsed Source* edited by R.J. Newport, B.D. Rainford and R. Cywinski (Hilger, Bristol, U.K., 1988), p. 324.
57. P.B. Lukins, D.R. McKenzie, A.M. Vassallo, and J.V. Hanna: C-13 NMR and FTIR study of thermal annealing of amorphous hydrogenated carbon. *Carbon* **31,** 569 (1993).
58. B. Dischler, A. Bubenzer, and P. Koidl: Bonding in hydrogenated hard carbon studies by optical spectroscopy. *Solid State Commun.* **48,** 105 (1983).
59. J. Gonzalez-Hernandez, B.S. Chao, and D.A. Pawlik: Characterization of as-prepared and annealed hydrogenated carbon-films. *J. Vac. Sci. Technol.* **7,** 2332 (1989).
60. N.V. Novikov, M.A. Voronkin, A.A. Smekhnov, N.I. Zaika, and A.P. Zakharchuk: Deposition by reactive ion-plasma sputtering and characterisation of C–N thin films. *Diamond Relat. Mater.* **4,** 390 (1995).